



Electrochemiluminescence energy transfer-promoted ultrasensitive immunoassay using near-infrared-emitting CdSeTe/CdS/ZnS quantum dots and gold nanorods

SUBJECT AREAS:

SENSORS

QUANTUM DOTS

FLUORESCENT PROBES

ENERGY TRANSFER

Received
21 January 2013

Accepted
7 March 2013

Published
25 March 2013

Correspondence and requests for materials should be addressed to J.-J.Z. (jjzhu@nju.edu.cn)

* These authors contributed equally to this work.

Lingling Li¹, Ying Chen^{1*}, Qian Lu^{1*}, Jing Ji^{1*}, Yuanyuan Shen¹, Mi Xu¹, Rong Fei¹, Guohai Yang¹, Kui Zhang², Jian-Rong Zhang¹ & Jun-Jie Zhu¹

¹State Key Laboratory of Analytical Chemistry for Life Science, Synergetic Innovation Center of Chemical Nature of Life Science, School of Chemistry and Chemical Engineering, Nanjing University, Nanjing 210093 (P. R. China), ²The Affiliated Drum Tower Hospital of Nanjing University Medical School, Nanjing 210008 (P. R. China).

The marriage of energy transfer with electrochemiluminescence has produced a new technology named electrochemiluminescence energy transfer (ECL-ET), which can realize effective and sensitive detection of biomolecules. To obtain optimal ECL-ET efficiency, perfect energy overlapped donor/acceptor pair is of great importance. Herein, we present a sensitive ECL-ET based immunosensor for the detection of tumor markers, using energy tunable CdSeTe/CdS/ZnS double shell quantum dots (QDs) and gold nanorods (GNRs) as the donor and acceptor, respectively. Firstly a facile microwave-assisted strategy for the synthesis of green- to near-infrared-emitting CdSeTe/CdS/ZnS QDs with time- and component-tunable photoluminescence was proposed. And, on the basis of the adjustable optical properties of both CdSeTe/CdS/ZnS QDs and GNRs, excellent overlap between donor emission and acceptor absorption can be obtained to ensure effective ECL-ET quenching, thus improving the sensing sensitivity. This method represents a novel approach for versatile detection of biomolecules at low concentrations.

The challenge for advanced biosensors is to detect biomolecules at low concentrations, which is crucially important for early-stage disease detection. Large numbers of nanomaterials with good fluorescence, electrochemical, surface-plasmon resonance properties have been adopted for biosensing applications¹⁻³. Among them, luminescence resonance energy transfer (LRET) is an attractive technique for the sensitive detection of biomolecules, which is a nonradiative process wherein a luminescent donor transfers energy to a proximal acceptor (luminescent or nonluminescent) via nonradiative dipole–dipole interactions^{4,5}. The rate of energy transfer is highly dependent on the extent of spectral overlap and the distance between the donor and acceptor⁴. According to the different types of the donor luminescence, mainly three kinds of LRET have been reported, namely fluorescence (or Förster) resonance energy transfer (FRET), chemiluminescence resonance energy transfer (CRET) and bioluminescence resonance energy transfer (BRET)⁵⁻⁷. Till now, there has been remarkable progress in the bioapplications of FRET, CRET and BRET⁸⁻¹⁰. Besides, as another kind of luminescence, electrochemiluminescence (ECL) has also attracted increasing interest in sensing applications due to its high sensitivity, wide dynamic concentration response range, as well as its potential and spatial controlment¹¹. Nevertheless, rare attention has been paid to the electrochemiluminescence based energy transfer (ECL-ET) as a result of the difficulty in finding a suitable donor/acceptor pair¹². To obtain optimal ECL-ET efficiency, perfect energy overlapped donor/acceptor pair is of great importance, therefore energy tunable materials are especially appealing as potential donor and acceptor. However, present works concerning ECL-ET are mostly comprised of non-adjustable donor or acceptor¹²⁻¹⁴. Consequently, the screening of ideal donor/acceptor pair for ECL-ET is a challenging work. Since the report of the ECL from Si quantum dots (QDs) by Ding and Bard in 2002, QDs have gradually become one of the most popular ECL species and been widely used for the construction of ECL



biosensors^{15–17}. Notably, the tunable emission wavelength and broad absorption spectra of QDs render them ideal active donor or acceptor for ECL-ET^{12,13}.

QDs with near-infrared (NIR) emission (650–900 nm) are particularly attractive, as biological autofluorescence and tissue absorption are both at their minima in this wavelength range^{18–20}. So far many kinds of NIR-emitting QDs have been reported, such as CdSeTe, InAs, PbSe, CdP and CuInS, etc^{21–25}, among which the alloyed CdSeTe QDs have been of immense interest since been reported in 2003²⁶. In comparison with other NIR-emitting QDs, alloyed CdSeTe QDs exhibit a very strong nonlinear effect between the composition and the absorption/emission energies, endowing them with special optical and electronic properties not available from the parent CdSe and CdTe QDs²⁶. Consequently, the emission wavelength of CdTeSe QDs can readily reach NIR region by tuning Te/Se molar ratio. Meanwhile, the parent CdSe QDs can only cover typically 480–620 nm in emission, and even the CdTe QDs of 7 nm can only reach ~720 nm in emission^{19,27,28}. To date, various methods have been developed for the synthesis of single or core-shell structured CdTeSe QDs^{20,28–32}. Nevertheless, most of these methods adopted high-temperature organometallic routes, and then additional complicated manipulations were required to disperse these QDs in water, leading to the decrease of quantum yield (QY) and the limitation for their further bioapplications^{19,33}.

On the other hand, it is well known that two prerequisites are necessary for the bioapplications of QDs, one is good optical properties such as strong fluorescence, high quantum yield and long lifetime, and the other is low biotoxicity. However, it has been reported that cadmium-based QDs pose risks to human health and the environment associated with the leaching of free Cd²⁺ ions from them via degradation, which will impede their biological applications. Fortunately, coating the cadmium-based core with proper shell, such as ZnS and polymer coatings, can repress the Cd²⁺ release and thus drastically reduce or even eliminate toxicity in vitro and in vivo^{34–36}. It is worth noting that, for the formation of “ideal” core-shell QDs, two criteria must be fulfilled. Firstly, the shell material should possess a much wider band gap than the core to suppress the exciton leakage into the shell. Secondly, the core and shell materials should have similar lattice parameters so that the shell-growth can happen in an epitaxial manner, without the formation of structural defects which could markedly lower the QY³⁷. Till now, the CdSeTe QDs are mostly passivated with nontoxic ZnS shell to obtain CdSeTe/ZnS coe-shell QDs. However, for both CdSe and CdTe, the large lattice mismatches (>10%) relative to ZnS hinder the formation of high-quality QDs. Therefore it is of high importance to develop new aqueous synthetic procedure for NIR-emitting core-shell CdTeSe QDs with excellent optical properties and low biotoxicity.

Besides, gold nanorods (GNRs) have attracted a great deal of attention due to their well-defined surface-plasmon based optical properties³⁸. GNRs possess two principal localized surface plasmon resonance (SPR) bands, namely, the transverse band and the longitudinal band (LSPR), corresponding to electron oscillations in the short and long axes of the GNRs, respectively. The former is located in the visible region around 520 nm, while the latter shows exquisite dependence on the aspect ratio with small variations (tunable from visible to NIR region) and without the need to significantly vary the overall dimensions^{38,39}. Such aspect ratio-dependent optical properties of the GNRs bring some advantages in a LRET system^{40,41}.

Herein, we propose the microwave-assisted production of high-quality NIR-emitting CdSeTe/CdS/ZnS QDs with successive epitaxial CdS and ZnS shells according to the relative lattice mismatches between each component as shown in Fig. 1. The double shelled CdSeTe/CdS/ZnS QDs possess exciting optical properties and favorable biocompatibility, showing valuable potential in bioapplications. The QDs are further used for the fabrication of a novel ECL-ET based

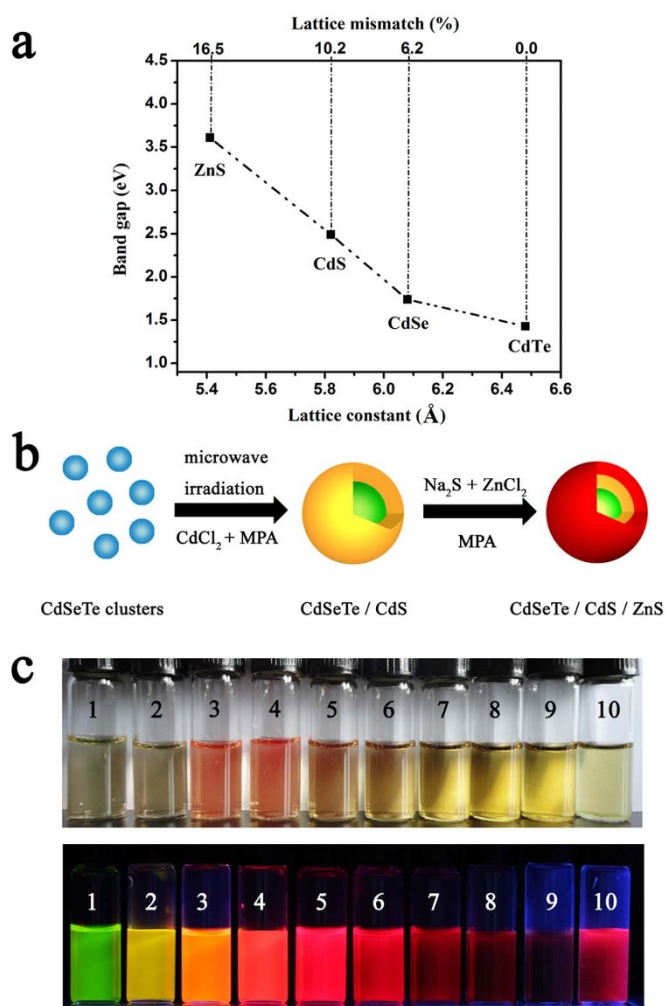


Figure 1 | Wavelength-tunable CdSeTe/CdS/ZnS QDs.

(a) Interrelationship between band gap energy, lattice constant, and lattice mismatch of bulk cubic CdTe, CdSe, CdS, and ZnS. Herein, lattice mismatch refers to the mismatch compared to CdTe. (b) Synthetic procedures for the preparation of CdSeTe/CdS/ZnS QDs. (c) Photo images of the prepared CdSeTe/CdS QDs (samples 1–9) and CdSeTe/CdS/ZnS QDs (sample 10, relative to sample 7) taken under visible (upper) and UV light (lower), respectively.

immunosensor, featuring perfect energy matched CdSeTe/CdS/ZnS QDs and gold nanorods (GNRs) as the donor-quencher pair. Greatly improved sensitivity is attained via twofold signal amplification from mesoporous SiO₂ coated carbon nanotubes (mCNTs)-QDs nanocomposites and ECL-ET technology. This approach provides a sensitive response to carcinoembryonic antigen (CEA) in a wide range from 0.001 to 200 pg mL⁻¹ with a detection limit of 0.0005 pg mL⁻¹. The proposed facile synthetic method for NIR-emitting QDs and novel ECL-ET signal amplification strategy should open exciting possibilities in developing advanced nanostructures and biosensors.

Results

Synthesis and characterization of CdSeTe/CdS/ZnS QDs. The small-sized CdSeTe clusters were firstly synthesized at low temperature under cadmium-rich condition, namely the cadmium precursor was about 20-fold in excess of the total amount of injected Se and Te (see Methods). Such cadmium-rich condition ensured the complete consumption of the injected Se and Te, the adequate reaction rate even at low temperature, as well as the formation of small sized production. 3-mercaptopropionic acid (MPA) was used as capping



agent and stabilizer, which attached onto QDs via a chemical bond between the metal atoms of QDs and the thiol groups of MPA. The UV-vis absorption spectra were explored for the preparation of the CdSeTe clusters at serial reaction time to monitor their size evolution (Supplementary Fig. S1). The results revealed that the reaction time of 1 h was sufficient for the growth of CdSeTe clusters, and prolonged reaction time could not cause obvious change in particle size.

To obtain CdSeTe based core-shell QDs with minimized toxicity and excellent photoluminescence (PL), CdSeTe/CdS/ZnS double shell QDs were designed according to the lattice mismatches between each relative component, namely CdSe, CdTe, CdS and ZnS as shown in Fig. 1a. The relatively small lattice mismatch between CdSe, CdTe and CdS ensures the epitaxial growth of CdS shell on the surface of CdSeTe QDs. Moreover, the small mismatch between CdS and ZnS lattice parameters enables the formation of core-shelled CdS/ZnS architecture with coherent epitaxial mode³³. Thus, the CdS shell can be expected to serve as a buffer layer between CdSeTe core and ZnS shell, allowing a stepwise change of lattice spacing for the resultant CdSeTe/CdS/ZnS QDs and reducing the strain inside the QDs (Fig. 1b).

The small-sized CdSeTe clusters were further used as the core for the subsequent one-pot facile synthesis of core-shell CdSeTe/CdS QDs with time- and component-tunable photoluminescence spanning both the visible and NIR regions (Fig. 1c). As the growth of the small-sized core and the coating of the shell took place simultaneously, overgrowth of the resultant CdSeTe/CdS QDs could be restrained, yielding smaller sized QDs with longer maximum emission wavelength compared with two-step synthetic approach.

The synthetic conditions for NIR-emitting CdSeTe/CdS QDs were optimized via investigating multiple parameters which influenced the optical properties of the QDs. Firstly the injected Te/Se molar ratio, with the constant concentration of Te precursor, is taken into consideration. A series of Te/Se molar ratios (100 : 0, 83 : 17, 75 : 25, 33 : 67 and 20 : 80) were selected and the result is displayed in Fig. 2a. It can be observed that, with increasing reaction time from 10 min to 30 min, the maximum emission wavelength of CdSeTe/CdS QDs red-shifts obviously with increasing Se amount at relatively low concentration. Such red-shift is an indication for the formation of expected CdSeTe/CdS core-shell structure rather than a CdSe_xTe_yS_{1-x-y} alloyed structure^{33,42}. However, at higher concentration, increasing Se amount can conversely lead to much weaker red-shift of the emission wavelength over time. When Te/Se molar ratio was 83 : 17, the resultant QDs showed the most obvious red-shift in emission wavelength, thus 83 : 17 was selected as the optimum composition for the preparation of NIR-emitting QDs. Secondly, with fixed Te/Se molar ratio of 83 : 17, the influence of the concentration of Cd precursor (CdCl₂) for CdS coating was also investigated. As shown in Fig. 2b, with the injection of individual MPA, the maximum emission wavelength of the resultant QDs has just negligible red-shift with the reaction time increased from 10 min to 30 min, indicating that the additional CdS shell is of great importance for the acquisition of NIR-emitting CdSeTe/CdS QDs. Furthermore, increasing CdCl₂ concentration resulted in gradual red-shift of CdSeTe/CdS QDs, and finally reaches the optimum condition at the concentration of 5 mM. High CdCl₂ concentration can lead to weaker emission red-shift of the resultant QDs, as well as in the PL intensity, probably because an excessively thick CdS shell can induce the formation of dislocations and new defects⁴².

To further confirm that the PL of CdSeTe/CdS QDs indeed originates from CdSeTe core, control experiment was carried out. When the individual CdS/MPA in the absence of CdSeTe core was radiated with microwave, the PL spectrum of the product was compared with that of the CdSeTe/CdS QDs (Supplementary Fig. S2). The negligible PL from CdS/MPA indicates that CdSeTe core is the optically active center in CdSeTe/CdS QDs.

The optical properties of the resulting CdSeTe/CdS QDs at different reaction time interval are depicted in Fig. 1c and Fig. 2c. As the reaction time prolonged from 2 min to 40 min, the absorption and PL wavelength red-shifted gradually (from 498 nm to 761 nm in emission), revealing the growth of the particles. It is noteworthy that the CdSeTe/CdS QDs can readily reach NIR region within just about 10 min. The CdSeTe/CdS QDs exhibited high QYs up to 56% with full-width at half maximum (FWHM) between 57~68 nm, which is much narrower than other reported NIR-emitting QDs, such as CdTe/CdSe QDs (70~80 nm), InAs (80~90 nm), Cd₃P₂ (75~100 nm), CuInS₂ (100~140 nm)^{22,23,25,43}. The high QYs and narrow spectral widths indicate that the alloyed QDs are highly crystalline in structure and monodispersed in solution.

The elemental composition of the resultant CdSeTe clusters and CdSeTe/CdS QDs prepared under the above mentioned optimum conditions were tested by ICP-AES and compared with the composite ratio of the injected precursors (Supplementary Table S1). The Te/Se molar ratio was almost unchanged, indicating the cadmium-rich condition could promote the complete consumption of the injected Se and Te.

In view of the inherent toxicity of the cadmium, an additional nontoxic ZnS shell was coated onto the CdSeTe/CdS QDs to minimize the toxicity of NIR-emitting QDs. The CdSeTe/CdS/ZnS QDs, in comparison with CdSeTe/CdS QDs, showed slight enhancement and red-shift in their PL behavior (Fig. 2d), suggesting that the CdSeTe/CdS QDs have not obvious surface defects after the passivation of CdS shell. Nevertheless, the CdSeTe/CdS/ZnS QDs possessed extended PL lifetime. As shown in Fig. 2e, the double shell QDs with a maximum emission wavelength of 648 nm and 764 nm have average lifetimes of 67 ns and 40 ns respectively, much longer than previously reported CdSeTe QDs³⁹. The detailed PL lifetime parameters were listed in the Supplementary Table S2^{29,44,45}.

The topographies and structures of the obtained CdSeTe nano-clusters, CdSeTe/CdS QDs, and CdSeTe/CdS/ZnS QDs were further characterized by high resolution transmission electron microscopy (HRTEM) images and X-ray powder diffraction (XRD) pattern as shown in Fig. 3. The CdSeTe clusters were confirmed to be subnanometer-sized with mean diameter of 1.5 nm. After microwave radiated for 40 min, the resultant CdSeTe/CdS QDs (λ_{em} : 761 nm) showed increased average size of 3.0 nm, and the mean size of the corresponding CdSeTe/CdS/ZnS QDs (λ_{em} : 764 nm) increased to 4.2 nm, indicating the thickness of 1.5 or 1.2 nm for the CdS or ZnS shell, respectively. It is worthy of note that the CdSeTe/CdS/ZnS QDs showed obvious lattice planes that stretched straight across the entire particle without evidence of an interface between the core and shells, implying a coherent epitaxial mechanism for the growth of both CdS and ZnS shells and demonstrating that the shell growth does not disturb the crystalline of the CdSeTe core^{33,42,46}. Moreover, the XRD patterns showed that CdSeTe core had a zinc-blende crystal structure. In contrast, the diffraction patterns of CdSeTe/CdS QDs and CdSeTe/CdS/ZnS QDs moved slightly toward higher angles due to the formation of the CdS and ZnS shells. A brief summary of the optical and morphological parameters of QDs stated above is provided for clarity (Supplementary Table S3).

Research revealed that the leaching of toxic Cd²⁺ ions from QDs and their tendency to aggregate in living cells are two key factors that lead to their cytotoxicity³³. Thus the dispersibility and stability of the water-soluble QDs under biologically relevant condition have been investigated (Supplementary Fig. S3). The results revealed that the QDs were not susceptible to aggregation in biologically relevant conditions. The bioactivity of CdSeTe/CdS/ZnS QDs was evaluated by MTT test and cell imaging as shown in Supplementary Fig. S4 and S5, verifying that such double shell NIR-emitting QDs had low toxicity and showed great possibility for targeted cell imaging.

In comparison with commercially available quantum dots (Supplementary Information), the CdSeTe/CdS/ZnS QDs display some

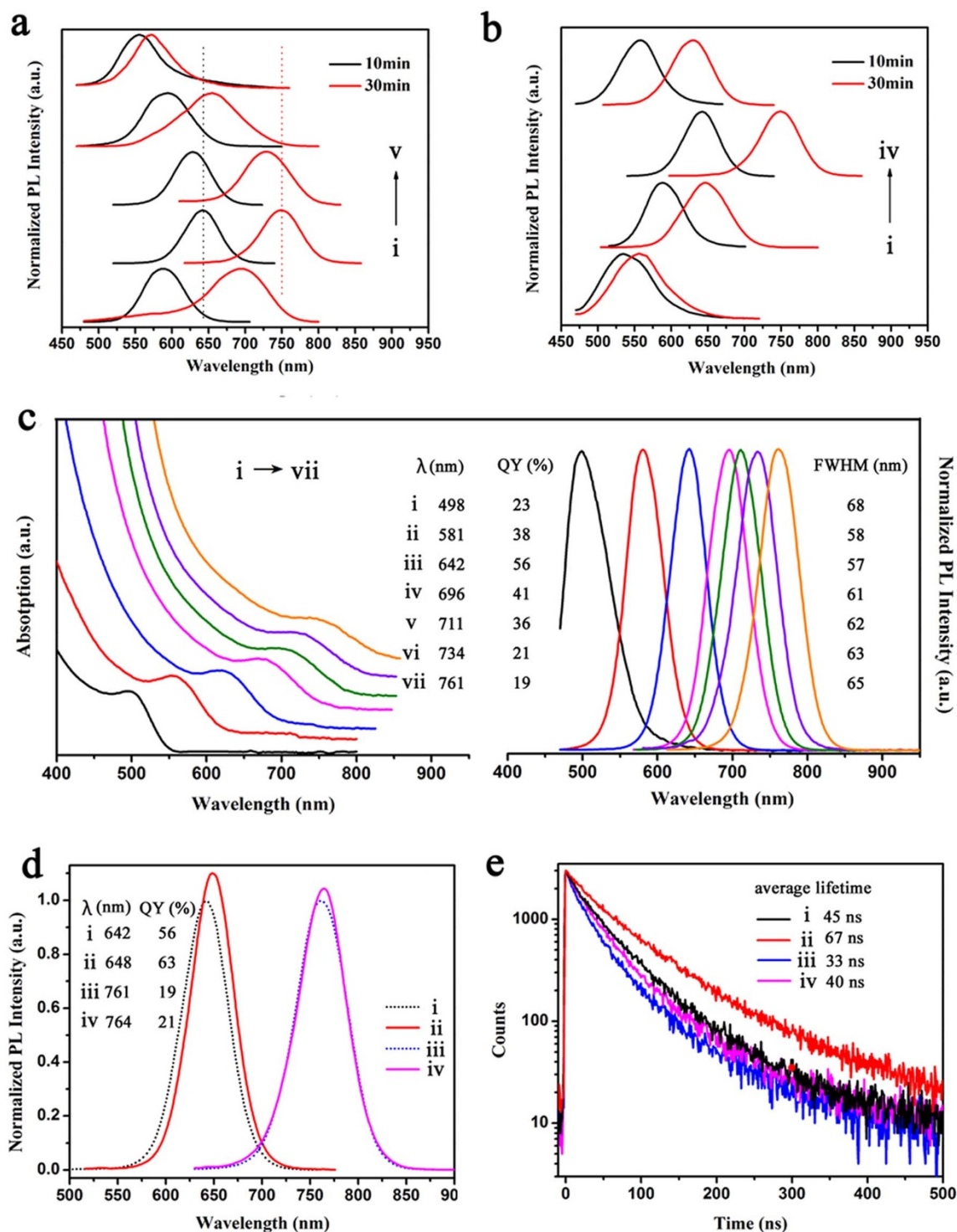


Figure 2 | Optical characterization of QDs. (a) Normalized PL spectra of CdSeTe/CdS QDs with variant Te/Se molar ratios after microwave radiated for 10 min and 30 min: (i) 100:0, (ii) 83:17, (iii) 75:25, (iv) 33:67, (v) 20:80. (b) Normalized PL spectra of CdSeTe/CdS QDs with different CdCl₂ concentrations (mM) for CdS coating: (i) 0, (ii) 2.5, (iii) 5, (iv) 10. (c) UV-vis absorption spectra (left) and PL (right) of the CdSeTe/CdS QDs prepared under the optimum reaction conditions with continuous reaction time: (i) 2 min, (ii) 5 min, (iii) 10 min, (iv) 15 min, (v) 20 min, (vi) 25 min, (vii) 40 min. And the related emission wavelength, QYs and FWHM values are presented. (d, e) PL (d) and lifetime spectra (e) of the CdSeTe/CdS QDs (i and iii) and corresponding CdSeTe/CdS/ZnS QDs (ii and iv), as well as the related emission wavelength, QYs, average lifetimes.

attractive virtues, such as smaller size, longer lifetime, and narrower FWHM in the NIR region. Moreover, only few emission wavelengths of commercial quantum dots could be purchased. Contrarily, by using the proposed synthetic procedure, the researchers can easily obtain quantum dots with various colors for different applications, making the CdSeTe/CdS/ZnS QDs remarkably attractive.

Characterization of the ECL-ET donor-quencher pair. CNTs have been widely used for signal amplification in ECL sensing research due to their excellent conductivity, large specific surface area, and good biocompatibility^{16,47}. However, on the other hand, CNTs can absorb the emission from both PL and ECL of QDs because of energy transfer and blackbody effect^{47–49}. As a consequence, both intense

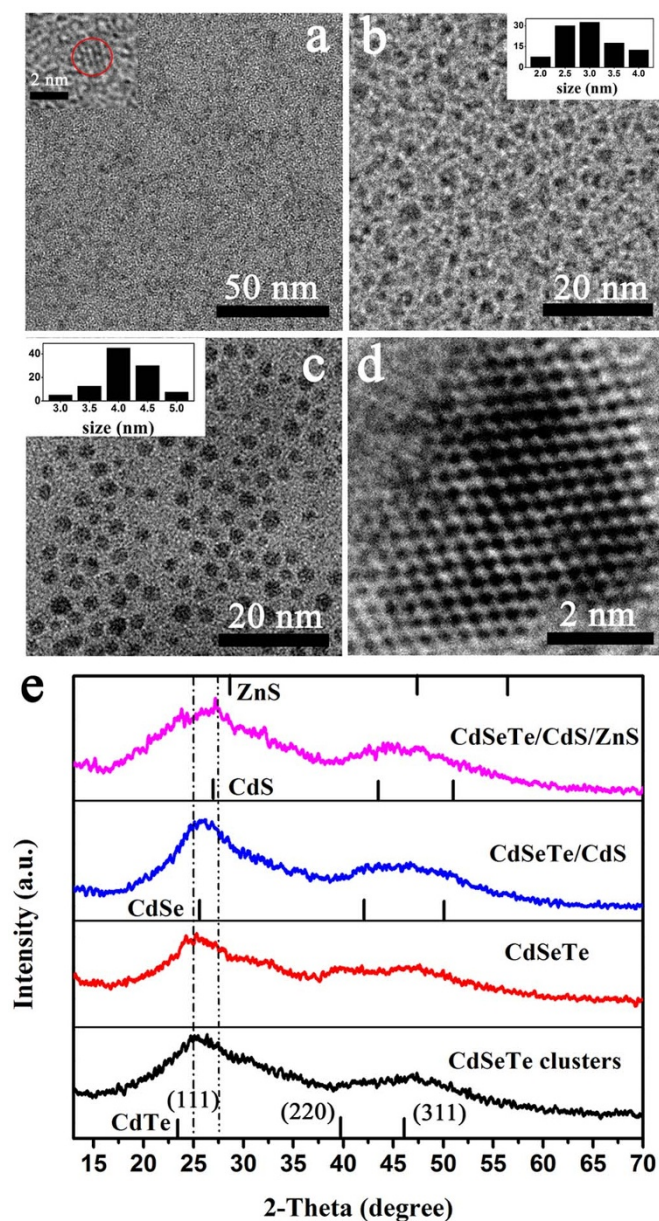


Figure 3 | Topography and structure evolution upon QDs synthesis. (a–d) HRTEM images of CdSeTe clusters (a), CdSeTe/CdS QDs (b), and CdSeTe/CdS/ZnS QDs (c, d). The inset in (a) depicts the representative image of individual CdSeTe nanoclusters, the insets in (b) and (c) represent the size distributions of the corresponding QDs. (e) XRD patterns of CdSeTe nanoclusters, CdSeTe QDs, CdSeTe/CdS QDs, and corresponding CdSeTe/CdS/ZnS QDs. Standard diffraction lines of cubic CdTe, cubic CdSe, cubic CdS, and cubic ZnS are shown for comparison.

enough ECL signal and low ECL absorption in CNTs-QDs composites must be satisfied to rule out the interference of CNTs and finally ensure high ECL-ET efficiency. It is reported that deposition of a silica spacer between the QDs and the CNTs can minimize the PL quenching more effectively than polymer-wrapping technique⁴⁸. Given the above situations, we chose to coat CNTs with a mesoporous SiO₂ layer to hinder light quenching as much as possible and meanwhile minimize adverse effects arising from the insulativity of silica (Fig. 4a and Supplementary Methods). As depicted in Supplementary Fig. S6, the CNTs with a mesoporous SiO₂ coating (mCNTs) showed a diameter of 40 nm, much larger than that of acid treated CNTs (ca. 20 nm), therefore the thick of silica coating layer was about 10 nm. The NIR-emitting CdSeTe/CdS/ZnS

QDs with a maximum emission wavelength of 711 nm (QDs711) were conjugated to mCNTs with cationic polyelectrolyte PEI as the binding linker via the formation of an amide bond between amino groups in PEI and carboxyl groups of MPA attached on QDs surface (Supplementary Fig. S7), as well as electrostatic interactions between positively charged PEI and negatively charged QDs. The successful conjugation of PEI with mCNTs was verified by zeta potential (Supplementary Fig. S8). For comparison, PEI functionalized acid treated CNTs (pCNTs) were also prepared and conjugated with the same QDs. The PL intensity of mCNTs-QDs nanocomposites was 5.5 times higher than that of pCNTs-QDs nanocomposites (Supplementary Fig. S9), demonstrating that mesoporous SiO₂ coating could indeed inhibit PL quenching. Moreover, the maximum emission wavelength of QDs711 slightly red shifted to 718 nm (Fig. 5a), arising from a decrease of the quantum confinement of QDs after assembly onto CNTs⁴⁸.

As for the ECL-ET acceptor, the CTAB stabilized GNRs were treated with PSS and then conjugated with Ab₂ according to previous report (see Methods)⁵⁰. In order to obtain optimum ECL-ET, LSPR band of GNRs-Ab₂ bioconjugates must overlap with the ECL peak wavelength of QDs-mCNTs nanocomposites to the largest extent. Upon careful screening, the GNRs with LSPR band at 701 nm (GNRs701) were finally chosen as the optimal acceptor, the resultant GNRs-Ab₂ bioconjugates showed a red-shifted LSPR band at 724 nm, proximate with ECL peak wavelength of QDs-mCNTs nanocomposites at 726 nm (Fig. 5a).

Insights into the quenching mechanisms. As for the energy transfer process between a molecular dye as the donor and a metallic acceptor (such as metallic surface, metal nanoparticles, etc.), two cardinal mechanisms have been developed, that is FRET and nanometal surface energy transfer (NSET). Both FRET and NSET are through-space mechanism and their energy transfer efficiencies strongly depend on the separation distance between donor and acceptor⁵¹. The key differences are that FRET is a dipole-dipole type energy transfer with $1/r^6$ distance dependence, while NSET is a dipole-surface type energy transfer following $1/r^4$ distance dependence^{52–54}. To explore the mechanism of energy transfer in this work, we introduced a QDs-dsDNA-GNRs conjugate, which was composed of QDs682 as the donor, GNRs676 as the acceptor, and the rigid dsDNA as the spacer with length varying from 6.24 nm to 17.12 nm. QDs682

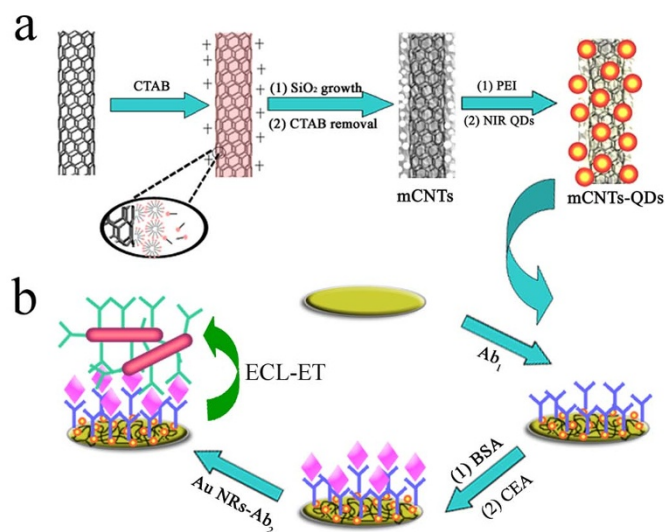


Figure 4 | Construction of the ECL immunosensor. (a) Schematic representation of preparation procedure for mCNTs-QDs composites. (b) Schematic illustration of the stepwise immunosensor fabrication process.

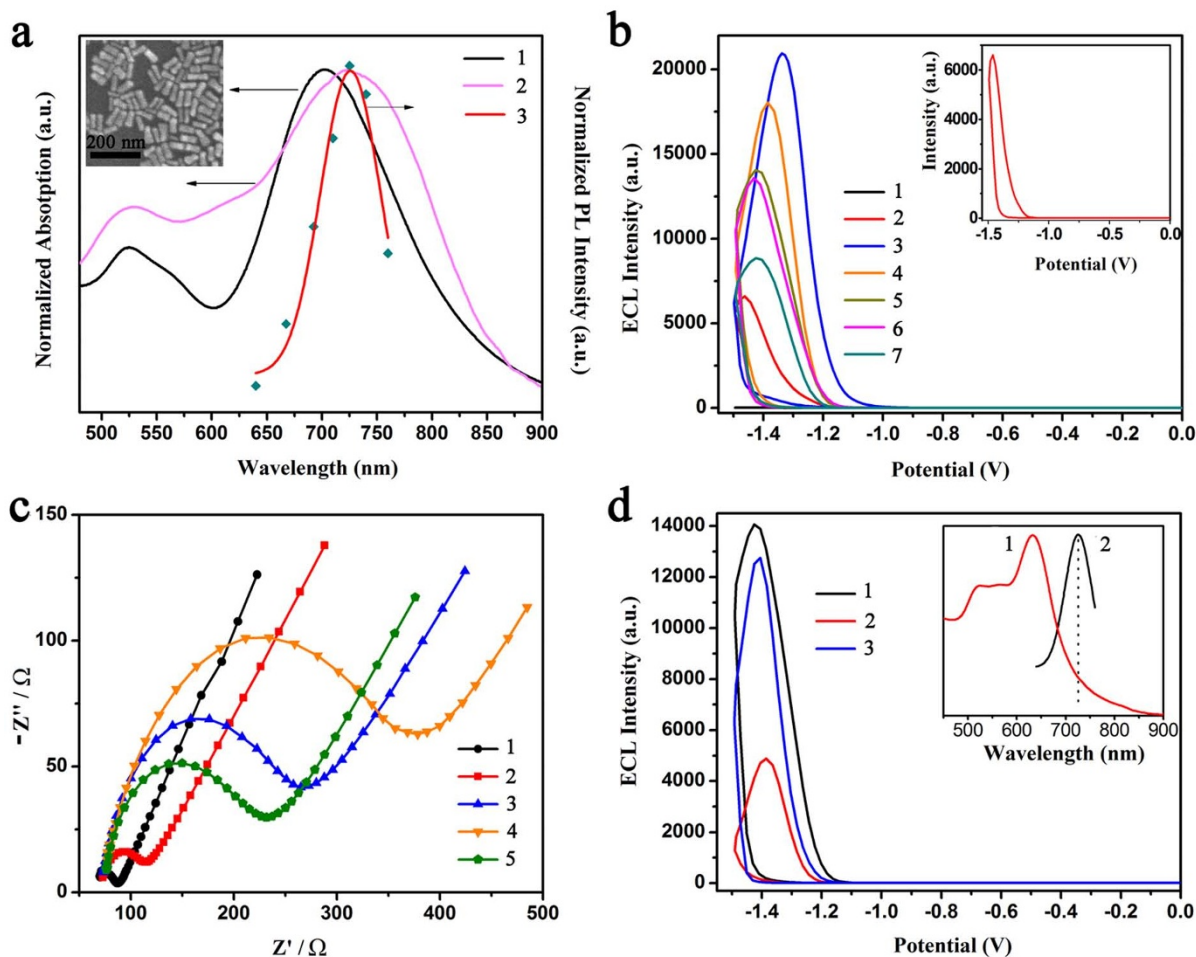


Figure 5 | The monitoring of the ECL-ET based sensor assembly. (a) Comparison of the spectral properties among QDs and GNRs based donor/acceptor pair. (1) and (2) are the UV-vis absorption spectra of GNRs and GNRs-Ab₂, respectively. (3) is the ECL spectrum of mCNTs-QDs nanocomposites. Inset is the SEM image of GNRs. (b) ECL – potential curves of stepwise modified electrodes: (1) bare GE, (2) pure QDs/GE, (3) mCNTs-QDs/GE, (4) mCNTs-QDs-Ab₁/GE, (5) BSA/mCNTs-QDs-Ab₁/GE, (6) CEA/BSA/mCNTs-QDs-Ab₁/GE, (7) GNRs-Ab₂/CEA/BSA/mCNTs-QDs-Ab₁/GE, here CEA concentration is 0.1 pg mL⁻¹. The inset is the separate ECL – potential curve of (2). (c) EIS of (1) GE, (2) mCNTs-QDs-Ab₁/GE, (3) BSA/mCNTs-QDs-Ab₁/GE, (4) CEA/BSA/mCNTs-QDs-Ab₁/GE, (5) GNRs-Ab₂/CEA/BSA/mCNTs-QDs-Ab₁/GE respectively, here CEA concentration is 5 pg mL⁻¹. (d) Influence of GNRs on the ECL-ET efficiency. (1) to (3) are BSA/mCNTs-QDs-Ab₁/GE, GNRs701-Ab₂/CEA/BSA/mCNTs-QDs-Ab₁/GE, and GNRs633-Ab₂/CEA/BSA/mCNTs-QDs-Ab₁/GE respectively, here CEA concentration is 10 pg mL⁻¹. Inset: comparison of (1) UV-vis absorption spectrum of GNRs633 and (2) ECL spectrum of mCNTs-QDs nanocomposites.

and GNRs676 were positioned at the opposite 5' ends of the dsDNA (Supplementary Fig. S10). Thus a plot of the quenching efficiency versus separation distance could be obtained. Supplementary Fig. S12b compared the experimentally observed quenching efficiencies with the theoretical energy transfer efficiency curves based on FRET and NSET models, where the Förster radius (R_0) and NSET radius (d_0) are calculated to be 124 Å and 74 Å, respectively. The results indicated that the experimental data was between FRET and NSET theoretical curves, specifically, it was more close to the FRET curves at long separations, but deviated from FRET behavior towards NSET behaviour at short separations. This is quite possibly because the asphericity and large size of the GNRs can lead to the breaking down of the point-dipole approximation (see Supplementary Information) at distance comparable to the radius of the metal nanoparticle, and the distance dependence of energy transfer is strongly influenced by the relative orientation⁵⁵. Besides, at shorter distances electron transfer may give rise to additive nonradiative decay transfer between the QDs and the metal surface⁵⁶. Thus it is not sufficiently accurate to conclude that the quenching mechanism is solely based on FRET or NSET model in present system. Fortunately, for the energy transfer process, the quenching efficiency is

determined by the number of acceptor molecules interacting with one donor while the separation distance between donor and acceptor is fixed⁷, thus providing an effective strategy for quantitative determination^{57,58}. In other words, although the detailed quenching mechanism still requires further clarification, the feasibility of quantitative determination based on energy transfer process is theoretically valid. In present system, the separation distance is in fact the size of the sandwich-type antigen-antibody immune complex, therefore the quenching efficiency is relative to the CEA concentration, as a result, CEA can be quantitatively detected.

As for the energy transfer systems, the effective energy transfer distance can be estimated by the “rule of thumb” $R_0 \pm 50\% R_0$ for the upper and lower limits^{4,7,59,60}. To ensure that the distance between the QDs/GNRs donor/acceptor pair is effective for the occurrence of ECL-ET, we estimated the actual distance (r) between the donor and acceptor through HRTEM characterization. However, it was hard to get the r value from the HRTEM image of mCNTs-QDs-Ab₁/CEA/GNRs-Ab₂ nanocomposites due to the obstruction of mCNTs (Supplementary Fig. S13). Thus, we simplified the ECL-ET system by conjugating the QDs and GNRs via immunoreaction just without the mCNTs. As shown in Supplementary Fig. S14, the



construction of the resultant QDs-Ab₁/CEA/GNRs-Ab₂ nanocomposites was simulated and depicted, as well as the HRET images. The results indicated that all the QDs711 were in close proximity to GNRs, falling within the effective distance (R_0 for QDs711/GNRs701 donor/acceptor pair is calculated to be 147 Å).

Fabrication and characterization of the ECL immunosensor. As shown in Fig. 4b, for the fabrication of the ECL immunosensor, mCNTs-QDs-Ab₁ bioconjugates are firstly coated onto the electrode, after blocked with BSA, CEA and GNRs-Ab₂ bioconjugates are successively attached onto mCNTs-QDs-Ab₁ bioconjugates modified electrode through antigen-antibody specific recognition. Therefore the QDs/GNRs donor/acceptor pair was brought into close proximity, ECL-ET can occur and lead to the quenching of the QDs ECL (Fig. 6). The decrease extent is relative to the amount of acceptor (GNRs-Ab₂ bioconjugates), namely the CEA concentration, thus CEA can be quantitatively detected.

ECL signals at each immobilization steps were recorded to monitor the fabrication of the immunosensor. As shown in Fig. 5b, the bare gold electrode (GE) exhibits negligible ECL signal, and an intensive ECL emission peak around -1.46 V with an onset potential of -1.14 V can be obtained after the assembly of pure CdSeTe/Cds/ZnS QDs. Notably, the ECL intensity from the mCNTs-QDs composite film was about 3.2-fold higher than that observed from the pure QDs film, accompanying positively shifted emission peak at -1.33 V with an onset potential of -1.0 V. The results could be attributed to the presence of mCNTs which decreased the potential barriers of the ECL reaction, indicating that the mCNTs possessed excellent conductivity even after SiO₂ coating (Supplementary Fig. S15). In addition, the more porous structure and larger surface area in the composite film could not only provide more binding sites for the adsorption of QDs, but also facilitate the diffusion of ECL co-reactant K₂S₂O₈ into the membrane, thus amplifying the ECL signal⁶¹. The ECL signal from mCNTs-QDs-Ab₁ bioconjugates modified electrode was relatively weaker and negatively shifted (-1.39 V), ascribed to the insulativity of proteins. The following assembly of BSA could observably decrease the ECL signal, and the CEA (0.1 pg mL⁻¹) adsorption only led to slight ECL decrease. Nevertheless, after the GNRs-Ab₂ bioconjugates were loaded onto the mCNTs-QDs-Ab₁/BSA/CEA modified electrode, the ECL signal dropped severely with a quenching degree of 34.7%, providing strong evidence for the feasibility of ECL-ET. All the above results indicated the successful construction of ECL immunosensor.

Electrochemical impedance spectroscopy (EIS) analysis was performed to support the assembly as shown in Fig. 5c. After the mCNTs-QDs-Ab₁ bioconjugates were immobilized onto the electrode, the electron-transfer resistance (R_{et}) just increased somewhat in comparison with bare GE, suggesting the good conductivity of mCNTs even in the presence of silica coating. The conjugation of BSA and CEA resulted in the increase of R_{et} value due to their insulating properties^{16,62}. However, obviously decreased R_{et} could

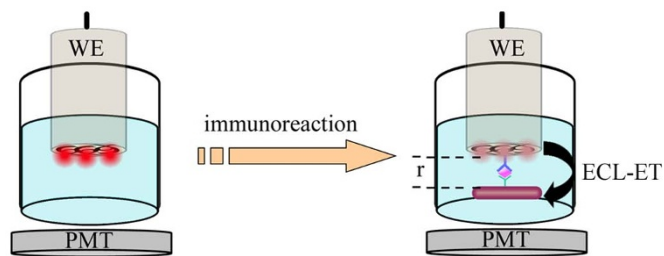


Figure 6 | ECL-ET model. Schematic representation of the ECL-ET between QDs/GNRs donor/acceptor pair located in close proximity via immunoreaction, wherein the ECL setup is curly represented by the electrolytic cell, the working electrode (WE) and the PMT.

be observed after the GNRs-Ab₂ bioconjugates were assembled onto the electrode, originating from the excellent conductivity of GNRs, which was further proved by cyclic voltammogram (CV) of the modified electrode before and after the assembly of GNRs-Ab₂ bioconjugates (Supplementary Fig. S16 and S17).

To demonstrate that the ECL signal decrease indeed arises from ECL-ET, GNRs with LSPR band at 633 nm (GNRs633) were prepared as the acceptor for parallel experiments. As shown in Fig. 5d, while GNRs701 could result in ECL quenching degree of 65.1% in the presence of 10 pg mL⁻¹ CEA, the GNRs633 could just lead to ECL quenching degree of 9.5%. The results proved that the energy overlap between the donor/acceptor pair was of great importance and the selected donor-acceptor herein could effectively ensure the occurrence of ECL-ET.

The effect of the QDs size on the ECL-ET efficiency was also taken into consideration. As stated above, the QDs prepared using the proposed synthetic approach possessed quite small size, which means that small variation in the size of QDs will leading to greatly shift of the emission wavelength. As shown in the Supplementary Fig. S18, the QDs570 exhibited mean diameter approximate to that of QDs764 (Fig. 3c). Such extreme variation in emission wavelength has a strong impact on the spectral overlap extent of the QDs and GNRs, thus affecting the ECL-ET efficiency.

CEA detection with the ECL immunosensor. The proposed immunosensor showed stable ECL signal upon consecutive potential scans (Supplementary Fig. S19), indicating the feasibility for ECL detection. As demonstrated above, after GNRs-Ab₂ bioconjugates were immobilized onto the electrode, the ECL intensity dramatically decreases due to the occurrence of ECL-ET. The higher CEA concentration could result in stronger ECL quenching, as a result, much weaker ECL signal could be observed. Fig. 7 illustrates the ECL responses of the immunosensor toward different concentrations of CEA and the corresponding standard calibration curve for CEA detection. The ECL signal decreased linearly with the increasing logarithmic value of CEA concentration in the range of 0.001~200 pg mL⁻¹, and the detection limit was 0.0005 pg mL⁻¹ using the signal to noise ratio S/N = 3. According to the linear equation, CEA could be detected quantitatively with the ECL immunosensor.

According to previous reports on ECL immunosensor, upon the conjugation of antigen onto the QDs and antibody modified electrode, the formation of antigen-antibody complex can lead to steric hindrance, as well as the increased electron-transfer resistance because of the insulating nature of proteins. Therefore electron- and mass-transfer are hindered, and the ECL signal decrease is relative to the antigen concentration to some extent^{63,64}. The comparison between antigen-antibody complex and ECL-ET based sensing strategies were also performed as shown in Fig. 7b. Obviously, the ECL-ET based strategy (mCNTs-QDs-Ab₁/BSA/CEA/GNRs-Ab₂) was much more sensitive for CEA detection and 200 pg mL⁻¹ CEA resulted in ECL quenching degree of 89.1%, whereas antigen-antibody complex (mCNTs-QDs-Ab₁/BSA/CEA) only led to slighter changes in ECL intensity below CEA concentration of 0.1 pg mL⁻¹. Above results revealed that the ECL-ET upon the introduction of GNRs-Ab₂ bioconjugates could effectively amplify the sensing signal and improve the detection sensitivity.

Specificity, reproducibility, and stability of the immunosensor.

Specificity is an important criterion for immunosensors. The potential interference from coexisting species toward CEA detection was studied by comparing the ECL response of the immunosensor toward pure CEA (10 pg mL⁻¹) and the mixture composed of CEA (10 pg mL⁻¹), alpha-fetal protein (50 pg mL⁻¹) and BSA (100 pg mL⁻¹). No significant difference (RSD 6.5%) was obtained, suggesting that the proposed immunosensor had a good specificity to CEA. Thus this immunosensor is feasible for the determination of CEA in human specimens.

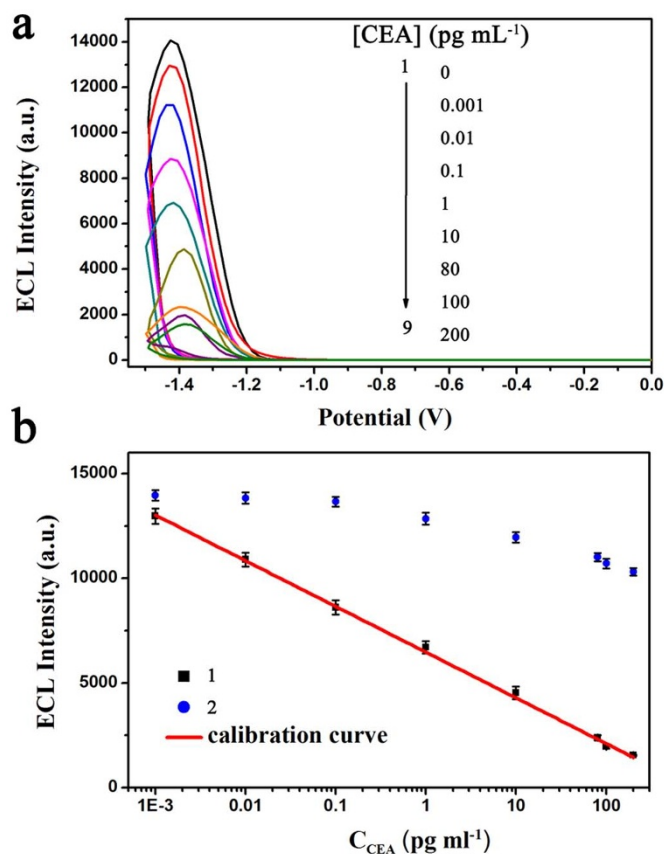


Figure 7 | Sensitive detection of CEA. (a) ECL–potential curves of the immunosensor at different concentrations of CEA. (b) Calibration curve for CEA determination using (1) ECL-ET and (2) antigen-antibody complex based sensing strategies, error bars were calculated from triple parallel experiments.

The reproducibility of the immunosensor for CEA detection was investigated through intra- and interassay precision, which were evaluated by measuring the same CEA sample with three reduplicate measurements, and with three immunosensors made on the same electrode. The intra- and interassay RSDs for 10 pg mL^{-1} CEA were 2.7% and 6.6% respectively, indicating the immunosensor had acceptable precision and fabrication reproducibility. After the immunosensor was stored in pH 7.4 PBS at 4°C for 20 days, no significant change was observed in the analytical performances for the same CEA concentration, which indicates that the immunosensor has good stability.

Measurement of CEA in human serum. The feasibility of the immunoassay for clinical applications was evaluated by comparing the assay results of clinical serum samples using the proposed ECL immunosensor with the traditional ELISA method. Three clinically acquired human serum samples with varying CEA content after an appropriate dilution with pH 7.4 PBS were tested. The results listed in Supplementary Table S4 showed an acceptable agreement, indicating the acceptable accuracy of the proposed sensor for the detection of CEA in clinical samples.

Discussion

Taken together, this work has introduced an integrated system ranging from the synthesis of near-infrared-emitting alloyed CdSeTe/CdS/ZnS double shell QDs to the fabrication of ECL-ET based biosensor with perfect energy matched donor/acceptor pair for sensitive detection of tumor markers (CEA). This work has several key meritorious novelties, including the appealing QDs synthetic approach,

the rigorous screening of donor/acceptor pair, and the extremely high sensitivity owing to multiplex signal amplification strategies. The synthesis of CdSeTe/CdS/ZnS double shell QDs follows coherent epitaxial shell growth mechanism, and the resultant QDs exhibit time- and component-tunable photoluminescence, excellent optical properties capable of competing with other kinds of near-infrared-emitting QDs, and favourable biocompatibility. This new class of QDs shows broad use in multicolor bioimaging, biosensing, and other biologic system. Moreover, taken advantage of the inherent energy tunable properties of both QDs and GNRs, perfectly energy matched CdSeTe/CdS/ZnS QDs and GNRs were selected and used as the donor/acceptor pair for the fabrication of ECL-ET based immunosensor. Greatly improved sensitivity was realized in this work via twofold signal amplification from mCNTs-QDs nanocomposites and ECL-ET technology. CEA in human serum was measured with this sensors with high accuracy compared to a referee ELISA method. It provides a novel class of signal amplification strategy for ECL immunosensing, and can be adopted easily for the detection of other proteins.

Methods

Chemicals and materials. Mouse monoclonal capture and signal anti-CEA antibodies (clone no. C3 and B5), Human alpha-fetal protein were purchased from Beijing Biosynthesis Biotechnology Co., Ltd. (Beijing, China). CEA standard solutions with concentrations from 0 to 400 ng mL^{-1} were from ELISA kits of CEA, which were supplied by Linc-Bioscience Co., Ltd. (Shanghai, China). Human IgG was purchased from Ningbo Xinzhi Biochemical Reagents (Ningbo, China). Polyethylenimine (PEI, 50%, w/w, in water, $M_w = 2,000$), Poly (sodium 4-styrenesulfonate) (PSS, 30%, w/w, in water, $M_w = 70,000$), and BSA (96–99%) were obtained from Sigma-Aldrich Chemical Co. (St. Louis, MO). Multiwalled CNTs (CVD method, purity $\geq 95\%$, diameter 10–30 nm, and length 5 μm) were purchased from Nanopoint. Co. Ltd. (Shenzhen, China). Ultrapure water obtained from a Millipore water purification system ($\geq 18 \text{ M}\Omega$, Milli-Q, Millipore) was used in all assays. The clinical serum samples were from Nanjing Drum Tower Hospital. All other reagents were of analytical grade and used as received without further purification.

Phosphate buffered saline (PBS) of various pH were prepared by mixing the stock solutions of NaH_2PO_4 and Na_2HPO_4 , and then adjusting the pH with 0.1 M NaOH and H_3PO_4 . The washing buffer was PBS (0.01 M, pH 7.4) containing 0.05% (w/v) Tween 20 (PBST). Blocking solution was PBS (0.01 M, pH 7.4) with 2% (w/v) BSA. 0.1 M PBS (pH 7.4) containing 0.1 M $\text{K}_2\text{S}_2\text{O}_8$ and 0.1 M KCl was used as the electrolyte in ECL analysis. 10 mM PBS (pH 7.4) containing 2.5 mM $[\text{Fe}(\text{CN})_6]^{3-/4-}$ and 0.1 M KCl was used for electrochemical impedance spectroscopy measurement.

Apparatus. The microwave synthesis of quantum dots was performed on a WBFY-201 Microwave Oven equipped with atmospheric reflux device (Nanjing Keer Instrument Equipments Co. Ltd., Nanjing, China). The ECL emission was detected with a Model MPI-A Electrochemiluminescence Analyzer (Xi'An Remax Electronic Science & Technology Co. Ltd., Xi'An, China). The voltage of the PMT was 600 V with 2 times of magnification in the detection process. The ECL spectrum was obtained by collecting the ECL peak intensity during the cyclic potential sweep with a series of optical filters (at 600, 630, 650, 685, 700, 720, and 760 nm) placed between the electrolytic cell and the PMT. The visual setup of the ECL instrument was presented in the Supplementary Fig. S20.

Synthesis of CdSeTe/CdS core-shell quantum dots. Our strategy for the preparation of the core, alloyed CdSeTe nanocluster was inspired by the method for small-sized CdTe core as originally presented by Liu et al.⁶⁵. In a typical synthesis, N_2 -saturated CdCl_2 solution (5 mM, 50 mL) containing 3-mercaptopropionic acid (MPA, 37 μL) at pH 12.2 was prepared at low temperature ($<20^\circ\text{C}$). Then premixed solutions of freshly prepared NaHTe and NaHSe with various Te/Se molar ratios (100 : 0, 83 : 17, 75 : 25, 33 : 67 and 20 : 80) were added into the CdCl_2 solution individually. Under these conditions, the cadmium precursor was about 20-fold in excess of the total amount of injected Se and Te (0.25 mM in total). The high Cd/(Te + Se) ratio can promote the growth of small-sized CdSeTe clusters. After stirring for 1 h, the expected CdSeTe clusters with diameters of about 1.5 nm were formed and stored in the refrigerator at 4°C for use (Fig. 3a).

For the synthesis of CdSeTe/CdS core-shell quantum dots, the CdSeTe clusters were precipitated with ethanol and collected via centrifugation at 6,000 rpm, then redissolved in 50 mL ultrapure water. CdCl_2 (5 mM) and MPA (40 μL) were added into the solution, the pH was tuned to 12.2 with 1 M NaOH. Then the CdSeTe/CdS precursor was irradiated and refluxed under microwave for different time. Aliquots of the reaction mixture were taken out periodically for UV and PL detection (Fig. 2). No post-preparative treatment was performed on the samples used for optical characterizations. Furthermore, in order to explore the influence of CdS shell on the CdSeTe/CdS quantum dots, various concentrations of CdCl_2 /MPA (with molar ratio 1 : 1.7) or individual MPA were also adopted for comparison. These as-prepared



CdSeTe/CdS quantum dots could be purified by precipitation and centrifugation. The precipitate was redissolved in 50 mL ultrapure water and used as CdSeTe/CdS core-shell quantum dots (200 nM) in subsequent steps for CdSeTe/CdS/ZnS core-shell-shell quantum dots.

Synthesis of CdSeTe/CdS/ZnS double shell quantum dots. Typical synthetic procedure for CdSeTe/CdS/ZnS quantum dots is as follows. MPA (20 μL) and ZnCl_2 solution (400 μL , 10 mM) were added into N_2 -saturated CdSeTe/CdS solution (pH 11.5). Then 500 μL Na_2S solution (10 mM) was added dropwise under stirring at 60°C. After stirring for 1 h, CdSeTe/CdS/ZnS core-shell-shell quantum dots were obtained.

The quantum yields (QYs) were estimated at room temperature using Rhodamine B, and Rhodamine 6G in ethanol according to the different maximum emission wavelengths of the quantum dots^{32,66}.

Preparation of the mCNTs-QDs-Ab₁ Bioconjugates. The mesoporous SiO_2 coated CNTs (mCNTs) were prepared according to previous report with small modification and further functionalized with PEI (Fig. 1a and Supplementary Methods)⁶⁷. To prepare mCNTs-QDs composites, the QDs were firstly purified and concentrated through ultrafiltration under centrifugation (3000 MW, 3000 rpm). Then 600 μL of purified QDs (500 nM) were first activated with 200 μL of freshly prepared 10 mg mL^{-1} EDC in 10 mM pH 7.4 PBS at room temperature for 20 min, followed by the addition of 200 μL of PEI functionalized mCNTs (0.5 mg mL^{-1}) with QDs/mCNTs volume ratio of 3:1. The mixture was incubated for 2 h at room temperature under shaking in the dark. The free nonconjugated QDs were removed by centrifugation at 6,000 rpm for 5 min and washed with PBS for 3 times. The product was redispersed in 400 μL of 10 mM pH 7.4 PBS, which was denoted mCNTs-QDs composites. For attachment of primary anti-CEA antibody (Ab_1), the mCNTs-QDs composites were re-activated with 100 μL of freshly prepared 10 mg mL^{-1} EDC at room temperature for 20 min, followed by the addition of 400 μL of 10 $\mu\text{g mL}^{-1}$ Ab_1 in pH 7.4 PBS. After 1 h incubation at room temperature under shaking, the mixture was further incubated at 4°C for 12 h. Afterwards the mixture was centrifuged and washed with pH 7.4 PBS alternately for 3 times remove any free Ab_1 . 400 μL of 10 mM pH 7.4 PBS was added to the bioconjugate precipitate collected, vortexed to form an homogeneous dispersion, and stored in refrigerator at 4°C.

Preparation of the GNRs-Ab₂ Bioconjugates. CTAB stabilized GNRs with different aspect ratios were firstly prepared according to previous reports with appropriate modifications (Supplementary Methods)^{50,68}. Subsequently, 100 μL of 30% PSS solution was added into the GNRs dispersion and sonicated for 3 h. After centrifuged and washed for 3 times to remove excess polyelectrolyte, the resulting precipitate was redispersed in 5 mL pH 7.4 PBS and mixed with 20 $\mu\text{g mL}^{-1}$ secondary anti-CEA antibody (Ab_2) in PBS solution with volume ratio of 1:1. After shaking for 1 h, the GNRs-Ab₂ bioconjugates were centrifuged and washed with pH 7.4 PBS twice to remove unbound antibodies, and dispersed in 5 mL 1% BSA in pH 7.4 PBS for another 1 h to block nonspecific binding. The BSA blocked GNRs-Ab₂ bioconjugates were washed with PBS and dispersed again in 5 mL PBS, vortexed to form an homogeneous dispersion, and stored in refrigerator at 4°C for the detection of CEA.

Preparation of the ECL Immunosensor. Optimized steps in the immunosensor preparation procedure were as follows:

- A gold electrode (GE) was polished carefully with 1.0, 0.3, and 0.05 μm alumina powder on fine abrasive paper sequentially and then washed ultrasonically in water and ethanol for a few minutes. Prior to use, the Au electrode was cleaned with freshly made piranha solution (98% H_2SO_4 :30% $\text{H}_2\text{O}_2 = 3:1$, v/v) for 10 min and cleaned thoroughly with water.
- After the electrode was rinsed thoroughly with water and allowed to dry at room temperature, mCNTs-QDs-Ab₁ bioconjugates solution (10 μL) was dropped onto the cleaned electrode at room temperature. After rinsed thoroughly with washing buffer, 10 μL of blocking solution with 2% (w/v) BSA was dropped on the mCNTs-QDs-Ab₁ bioconjugates modified GE at 37°C for 1 h to block non-specific binding sites of mCNTs-QDs-Ab₁ film.
- After thoroughly washing, the mCNTs-QDs-Ab₁ modified GE was soaking in 50 μL of CEA samples with different concentrations at 37°C for 1 h, followed by washing with PBST for 1 min.
- Then the electrode was secured in an inverted position and incubated in 50 μL of GNRs-Ab₂ bioconjugates solution at 37°C for 1 h, followed by thoroughly washing with PBST. The resulting electrode was stored in the refrigerator 4°C when not in use.

The experimental parameters including temperature and pH were all optimized by means of ECL experiments in 0.1 M pH 7.4 PBS containing 0.1 M $\text{K}_2\text{S}_2\text{O}_8$ and 0.1 M KCl in our previous method⁴⁸ except the incubation time for GNRs-Ab₂ bioconjugates (Supplementary Fig. S21).

ECL Immunosensor Detection of CEA. 0.1 M pH 7.4 PBS containing 0.1 M $\text{K}_2\text{S}_2\text{O}_8$ and 0.1 M KCl was used as the electrolyte in ECL analysis, where the $\text{K}_2\text{S}_2\text{O}_8$ was the coreactant, and it is not necessary to purge N_2 before the ECL measurement. ECL and CV signals were obtained simultaneously via cyclic voltammetry between 0 V and -1.5 V with a scan rate of 200 mV s^{-1} using a configuration consisting of bare or modified gold electrodes (4 mm in diameter) as working electrode, a platinum

counter electrode, and a saturated calomel electrode as the reference electrode. All potentials were quoted in this manuscript against this reference electrode.

- Reuel, N. F. *et al.* Transduction of Glycan–Lectin Binding Using Near-Infrared Fluorescent Single-Walled Carbon Nanotubes for Glycan Profiling. *J. Am. Chem. Soc.* **133**, 17923–17933 (2011).
- Jung, J. H., Cheon, D. S., Liu, F., Lee, K. B. & Seo, T. S. A Graphene Oxide Based Immuno-biosensor for Pathogen Detection. *Angew. Chem.* **122**, 5844–5847 (2010).
- Lu, D. *et al.* A Novel Nanoparticle-Based Disposable Electrochemical Immunosensor for Diagnosis of Exposure to Toxic Organophosphorus Agents. *Adv. Funct. Mater.* **21**, 4371–4378 (2011).
- Sapsford, K. E., Berti, L. & Medintz, I. L. Materials for Fluorescence Resonance Energy Transfer Analysis: Beyond Traditional Donor–Acceptor Combinations. *Angew. Chem. Int. Ed.* **45**, 4562–4589 (2006).
- Qin, G., Zhao, S., Huang, Y., Jiang, J. & Ye, F. Magnetic Bead-Sensing-Platform-Based Chemiluminescence Resonance Energy Transfer and Its Immunoassay Application. *Anal. Chem.* **84**, 2708–2712 (2012).
- James, J. R., Oliveira, M. I., Carmo, A. M., Iaboni, A. & Davis, S. J. A rigorous experimental framework for detecting protein oligomerization using bioluminescence resonance energy transfer. *Nat. Meth.* **3**, 1001–1006 (2006).
- Clapp, A. R. *et al.* Fluorescence Resonance Energy Transfer Between Quantum Dot Donors and Dye-Labeled Protein Acceptors. *J. Am. Chem. Soc.* **126**, 301–310 (2003).
- Algar, W. R. *et al.* Quantum Dots as Simultaneous Acceptors and Donors in Time-Gated Förster Resonance Energy Transfer Relays: Characterization and Biosensing. *J. Am. Chem. Soc.* **134**, 1876–1891 (2012).
- Carriba, P. *et al.* Detection of heteromerization of more than two proteins by sequential BRET-FRET. *Nat. Meth.* **5**, 727–733 (2008).
- Liu, X., Freeman, R., Golub, E. & Willner, I. Chemiluminescence and Chemiluminescence Resonance Energy Transfer (CRET) Aptamer Sensors Using Catalytic Hemin/G-Quadruplexes. *ACS Nano* **5**, 7648–7655 (2011).
- Xu, S., Liu, Y., Wang, T. & Li, J. Positive Potential Operation of a Cathodic Electrogenerated Chemiluminescence Immunosensor Based on Luminol and Graphene for Cancer Biomarker Detection. *Anal. Chem.* **83**, 3817–3823 (2011).
- Wu, M.-S., Shi, H.-W., Xu, J.-J. & Chen, H.-Y. CdS quantum dots/Ru(bpy)₃(2+) electrochemiluminescence resonance energy transfer system for sensitive cytosensing. *Chem. Commun.* **47**, 7752–7754 (2011).
- Wu, M.-S., Shi, H.-W., He, L.-J., Xu, J.-J. & Chen, H.-Y. Microchip Device with 64-Site Electrode Array for Multiplexed Immunoassay of Cell Surface Antigens Based on Electrochemiluminescence Resonance Energy Transfer. *Anal. Chem.* **84**, 4207–4213 (2012).
- Shan, Y., Xu, J. J. & Chen, H. Y. Electrochemiluminescence quenching by CdTe quantum dots through energy scavenging for ultrasensitive detection of antigen. *Chem. Commun.* **46**, 5079–5081 (2010).
- Jie, G. F., Liu, B., Pan, H. C., Zhu, J. J. & Chen, H. Y. CdS nanocrystal-based electrochemiluminescence biosensor for the detection of low-density lipoprotein by increasing sensitivity with gold nanoparticle amplification. *Anal. Chem.* **79**, 5574–5581 (2007).
- Jie, G. F. *et al.* Electrochemiluminescence immunosensor based on CdSe nanocomposites. *Anal. Chem.* **80**, 4033–4039 (2008).
- Yan, J. *et al.* Paper-Based Electrochemiluminescent 3D Immunodevice for Lab-on-Paper, Specific, and Sensitive Point-of-Care Testing. *Chem. Eur. J.* **18**, 4938–4945 (2012).
- Ma, Q. & Su, X. Near-infrared quantum dots: synthesis, functionalization and analytical applications. *Analyst* **135**, 1867–1877 (2010).
- Liang, G.-X. *et al.* Fabrication of near-infrared-emitting CdSeTe/ZnS core/shell quantum dots and their electrogenerated chemiluminescence. *Chem. Commun.* **46**, 2974–2976 (2010).
- Jiang, W., Singhal, A., Zheng, J., Wang, C. & Chan, W. C. W. Optimizing the Synthesis of Red- to Near-IR-Emitting CdS-Capped CdTeSe_{1-x} Alloyed Quantum Dots for Biomedical Imaging. *Chem. Mater.* **18**, 4845–4854 (2006).
- Allen, P. M. & Bawendi, M. G. Ternary I–III–VI Quantum Dots Luminescent in the Red to Near-Infrared. *J. Am. Chem. Soc.* **130**, 9240–9241 (2008).
- Xie, R., Rutherford, M. & Peng, X. Formation of High-Quality I–III–VI Semiconductor Nanocrystals by Tuning Relative Reactivity of Cationic Precursors. *J. Am. Chem. Soc.* **131**, 5691–5697 (2009).
- Miao, S., Hickey, S. G., Rellinghaus, B., Waurisch, C. & Eychmüller, A. Synthesis and Characterization of Cadmium Phosphide Quantum Dots Emitting in the Visible Red to Near-Infrared. *J. Am. Chem. Soc.* **132**, 5613–5615 (2010).
- Pietryga, J. M. *et al.* Utilizing the Lability of Lead Selenide to Produce Heterostructured Nanocrystals with Bright, Stable Infrared Emission. *J. Am. Chem. Soc.* **130**, 4879–4885 (2008).
- Allen, P. M. *et al.* InAs(ZnCdS) Quantum Dots Optimized for Biological Imaging in the Near-Infrared. *J. Am. Chem. Soc.* **132**, 470–471 (2009).
- Bailey, R. E. & Nie, S. M. Alloyed semiconductor quantum dots: Tuning the optical properties without changing the particle size. *J. Am. Chem. Soc.* **125**, 7100–7106 (2003).
- Taniguchi, S., Green, M., Rizvi, S. B. & Seifalian, A. The one-pot synthesis of core/shell/shell CdTe/CdSe/ZnSe quantum dots in aqueous media for in vivo deep tissue imaging. *J. Mater. Chem.* **21**, 2877–2882 (2011).



28. Pons, T. *et al.* Synthesis of Near-Infrared-Emitting, Water-Soluble CdTeSe/CdZnS Core/Shell Quantum Dots. *Chem. Mater.* **21**, 1418–1424 (2009).
29. Xing, B. *et al.* Highly-fluorescent alloyed quantum dots of CdSe_{1-x}Te_x synthesized in paraffin liquid: gradient structure and promising bio-application. *J. Mater. Chem.* **20**, 5664–5674 (2010).
30. Wang, R. *et al.* Homogeneously-Alloyed CdTeSe Single-Sized Nanocrystals with Bandgap Photoluminescence. *J. Phys. Chem. C* **113**, 3402–3408 (2009).
31. Wan, Z., Luan, W. & Tu, S.-T. Continuous synthesis of CdSe_xTe_{1-x} nanocrystals: Chemical composition gradient and single-step capping. *J. Colloid Interf. Sci.* **356**, 78–85 (2011).
32. Song, L., Duan, J. & Zhan, J. One-pot Microwave Assisted Synthesis of Homogeneously Alloyed CdSeTe_{1-x} Nanocrystals with Tunable Photoluminescence. *Mater. Lett.* **64**, 1843–1845 (2010).
33. He, Y. *et al.* Microwave synthesis of water-dispersed CdTe/CdS/ZnS core-shell quantum dots with excellent photostability and biocompatibility. *Adv. Mater.* **20**, 3416–3421 (2008).
34. Ye, L. *et al.* A pilot study in non-human primates shows no adverse response to intravenous injection of quantum dots. *Nat. Nano.* **7**, 453–458 (2012).
35. Derfus, A. M., Chan, W. C. W. & Bhatia, S. N. Probing the Cytotoxicity of Semiconductor Quantum Dots. *Nano Letters* **4**, 11–18 (2003).
36. Smith, W. E. *et al.* In Vitro Toxicity Assessment of Amphiphilic Polymer-Coated CdSe/ZnS Quantum Dots in Two Human Liver Cell Models. *ACS Nano* **6**, 9475–9484 (2012).
37. Reiss, P., Protière, M. & Li, L. Core/Shell Semiconductor Nanocrystals. *Small* **5**, 154–168 (2009).
38. Grzelczak, M. *et al.* Influence of Iodide Ions on the Growth of Gold Nanorods: Tuning Tip Curvature and Surface Plasmon Resonance. *Adv. Funct. Mater.* **18**, 3780–3786 (2008).
39. Wang, J. *et al.* Assembly of Aptamer Switch Probes and Photosensitizer on Gold Nanorods for Targeted Photothermal and Photodynamic Cancer Therapy. *ACS Nano* **6**, 5070–5077 (2012).
40. Xia, Y., Song, L. & Zhu, C. Turn-On and Near-Infrared Fluorescent Sensing for 2,4,6-Trinitrotoluene Based on Hybrid (Gold Nanorod)–(Quantum Dots) Assembly. *Anal. Chem.* **83**, 1401–1407 (2011).
41. Quach, A. D., Crivat, G., Tarr, M. A. & Rosenzweig, Z. Gold Nanoparticle–Quantum Dot–Polystyrene Microspheres as Fluorescence Resonance Energy Transfer Probes for Bioassays. *J. Am. Chem. Soc.* **133**, 2028–2030 (2011).
42. He, Y. *et al.* Microwave-Assisted Growth and Characterization of Water-Dispersed CdTe/CdS Core–Shell Nanocrystals with High Photoluminescence. *J. Phys. Chem. B* **110**, 13370–13374 (2006).
43. Kim, S., Fisher, B., Eisler, H.-J. & Bawendi, M. Type-II Quantum Dots: CdTe/CdSe(Core/Shell) and CdSe/ZnTe(Core/Shell) Heterostructures. *J. Am. Chem. Soc.* **125**, 11466–11467 (2003).
44. Tian, J. *et al.* Synthesis of CdTe/CdS/ZnS quantum dots and their application in imaging of hepatocellular carcinoma cells and immunoassay for alpha fetoprotein. *Nanotechnology* **21**, 305101 (2010).
45. Zeng, Q. *et al.* Synthesis and Optical Properties of Type II CdTe/CdS Core/Shell Quantum Dots in Aqueous Solution via Successive Ion Layer Adsorption and Reaction. *J. Phys. Chem. C* **112**, 8587–8593 (2008).
46. Talapin, D. V. *et al.* CdSe/CdS/ZnS and CdSe/ZnSe/ZnS Core–Shell–Shell Nanocrystals. *J. Phys. Chem. B* **108**, 18826–18831 (2004).
47. Wang, X.-F., Zhou, Y., Xu, J.-J. & Chen, H.-Y. Signal-On Electrochemiluminescence Biosensors Based on CdS–Carbon Nanotube Nanocomposite for the Sensitive Detection of Choline and Acetylcholine. *Adv. Funct. Mater.* **19**, 1444–1450 (2009).
48. Grzelczak, M. *et al.* Photoluminescence Quenching Control in Quantum Dot–Carbon Nanotube Composite Colloids Using a Silica-Shell Spacer. *Adv. Mater.* **18**, 415 (2006).
49. Pan, B. F. *et al.* Effects of Carbon Nanotubes on Photoluminescence Properties of Quantum Dots. *J. Phys. Chem. C* **112**, 939–944 (2008).
50. Wang, C., Chen, Y., Wang, T., Ma, Z. & Su, Z. Biorecognition-driven self-assembly of gold nanorods: A rapid and sensitive approach toward antibody sensing. *Chem. Mater.* **19**, 5809–5811 (2007).
51. Yun, C. S. *et al.* Nanometal Surface Energy Transfer in Optical Rulers, Breaking the FRET Barrier. *J. Am. Chem. Soc.* **127**, 3115–3119 (2005).
52. Jennings, T. L., Singh, M. P. & Strouse, G. F. Fluorescent Lifetime Quenching near $d = 1.5$ nm Gold Nanoparticles: Probing NSET Validity. *J. Am. Chem. Soc.* **128**, 5462–5467 (2006).
53. Singh, M. P. & Strouse, G. F. Involvement of the LSPR Spectral Overlap for Energy Transfer between a Dye and Au Nanoparticle. *J. Am. Chem. Soc.* **132**, 9383–9391 (2009).
54. Li, M. *et al.* Size-Dependent Energy Transfer between CdSe/ZnS Quantum Dots and Gold Nanoparticles. *J. Phys. Chem. Lett.* **2**, 2125–2129 (2011).
55. Saini, S., Srinivas, G. & Bagchi, B. Distance and Orientation Dependence of Excitation Energy Transfer: From Molecular Systems to Metal Nanoparticles. *J. Phys. Chem. B* **113**, 1817–1832 (2009).
56. Gueroui, Z. & Libchaber, A. Single-Molecule Measurements of Gold-Quenched Quantum Dots. *Phys. Rev. Lett.* **93**, 166108 (2004).
57. Liu, D. *et al.* Highly Robust, Recyclable Displacement Assay for Mercuric Ions in Aqueous Solutions and Living Cells. *ACS Nano* **6**, 10999–11008 (2012).
58. Wu, B.-Y., Wang, H.-F., Chen, J.-T. & Yan, X.-P. Fluorescence Resonance Energy Transfer Inhibition Assay for α -Fetoprotein Excreted during Cancer Cell Growth Using Functionalized Persistent Luminescence Nanoparticles. *J. Am. Chem. Soc.* **133**, 686–688 (2010).
59. Alam, R., Fontaine, D. M., Branchini, B. R. & Maye, M. M. Designing Quantum Rods for Optimized Energy Transfer with Firefly Luciferase Enzymes. *Nano Lett.* **12**, 3251–3256 (2012).
60. Freeman, R., Liu, X. Q. & Winner, I. Chemiluminescent and Chemiluminescence Resonance Energy Transfer (CRET) Detection of DNA, Metal Ions, and Aptamer-Substrate Complexes Using Hemin/G-Quadruplexes and CdSe/ZnS Quantum Dots. *J. Am. Chem. Soc.* **133**, 11597–11604 (2011).
61. Chen, L.-Y., Chen, C.-H., Tseng, C.-H., Lai, F.-L. & Hwanga, B.-J. Synthesis of CdSe(x)S(1-x) core/shell type quantum dots via one injection method. *Chem. Commun.* **47**, 1592–1594 (2011).
62. Liang, G., Shen, L., Zou, G. & Zhang, X. Efficient Near-Infrared Electrochemiluminescence from CdTe Nanocrystals with Low Triggering Potential and Ultrasensitive Sensing Ability. *Chem-Eur J* **17**, 10213–10215 (2011).
63. Jie, G., Wang, L. & Zhang, S. Magnetic Electrochemiluminescent Fe₃O₄/CdSe–CdS Nanoparticle/Polyelectrolyte Nanocomposite for Highly Efficient Immunosensing of a Cancer Biomarker. *Chem-Eur J* **17**, 641–648 (2011).
64. Jie, G.-F., Liu, P. & Zhang, S.-S. Highly enhanced electrochemiluminescence of novel gold/silica/CdSe–CdS nanostructures for ultrasensitive immunoassay of protein tumor marker. *Chem. Commun.* **46**, 1323–1325 (2010).
65. Deng, Z. *et al.* Aqueous Synthesis of Zinc Blende CdTe/CdS Magic-Core/Thick-Shell Tetrahedral-Shaped Nanocrystals with Emission Tunable to Near-Infrared. *J. Am. Chem. Soc.* **132**, 5592–5593 (2010).
66. Li, M. *et al.* Size-Dependent Energy Transfer between CdSe/ZnS Quantum Dots and Gold Nanoparticles. *J. Phys. Chem. Lett.* **2**, 2125–2129 (2011).
67. Kunlun, D. *et al.* A simple route to coat mesoporous SiO₂ layer on carbon nanotubes. *J. Mater. Chem.* **19**, 3725–3731 (2009).
68. Wang, C. G., Wang, T. T., Ma, Z. F. & Su, Z. M. pH-tuned synthesis of gold nanostructures from gold nanorods with different aspect ratios. *Nanotechnology* **16**, 2555–2560 (2005).

Acknowledgements

The authors thank the National Basic Research Program of China (2011CB933502) and the National Natural Science Foundation of China (21020102038, 21121091, 21175065, and 21103088) for financial support. This work is also supported by the Postdoctoral Science Foundation of China (No 2012M521039) and Jiangsu Planned Projects for Postdoctoral Research Funds (1201001B). The authors also thank Professor Nongjian Tao from Arizona State University for helpful discussions.

Author contributions

L.L., Y.S., M.X., J.-J.Z., designed the experiments. Y.C. and Y.S. prepared the gold nanorods. Q.L. and J.J. performed quantum dots synthesis. L.L. and M.X. carried out the fabrication and assays of sensors. R.F. and G.Y. assisted in the material characterizations. K.Z. performed the ELISA assay. L.L. analysed the data and wrote the paper, J.-J.Z. and J.-R.Z. revised the paper. All authors discussed and commented on the manuscript.

Additional information

Supplementary information accompanies this paper at <http://www.nature.com/scientificreports>

Competing financial interests: The authors declare no competing financial interests.

License: This work is licensed under a Creative Commons Attribution-NonCommercial-NoDerivs 3.0 Unported License. To view a copy of this license, visit <http://creativecommons.org/licenses/by-nc-nd/3.0/>

How to cite this article: Li, L. *et al.* Electrochemiluminescence energy transfer-promoted ultrasensitive immunoassay using near-infrared-emitting CdSeTe/CdS/ZnS quantum dots and gold nanorods. *Sci. Rep.* **3**, 1529; DOI:10.1038/srep01529 (2013).